Synchronization of Lorenz-Based Chaotic Circuits with Applications to Communications

Kevin M. Cuomo, *Member, IEEE*, Alan V. Oppenheim, *Fellow, IEEE*, and Steven H. Strogatz

Abstract— **A circuit implementation of the chaotic Lorenz system is described. The chaotic behavior of the circuit closely matches the results predicted by numerical experiments. Using the concept of synchronized chaotic systems (SCS's), two possible approaches to secure communications are demonstrated with the Lorenz circuit implemented in both the transmitter and receiver. In the first approach, a chaotic masking signal is added at the transmitter to the message, and at the receiver, the masking is regenerated and subtracted from the received signal. The second approach utilizes modulation of the coefficients of the chaotic system in the transmitter and corresponding detection of synchronization error in the receiver to transmit binary-valued bit streams.**

The use of SCS's for communications relies on the robustness of the synchronization to perturbations in the drive signal. As a step toward further understanding the inherent robustness, we establish an analogy between synchronization in chaotic systems, nonlinear observers for deterministic systems, and state estimation in probabilistic systems. This analogy exists because SCS's can be viewed as performing the role of a nonlinear state space observer. To calibrate the robustness of the Lorenz SCS as a nonlinear state estimator, we compare the performance of the Lorenz SCS to an extended Kalman filter for providing state estimates when the measurement consists of a single noisy transmitter component.

I. Introduction

CHAOTIC systems provide a rich mechanism for signal design and generation, with potential applications to communications and signal processing. Because chaotic signals are typically broadband, noiselike, and difficult to predict, they can be used in various contexts for masking information-bearing waveforms. They can also be used as modulating waveforms in spread spectrum systems.

A particularly useful class of chaotic systems are those that possess a self-synchronization property [1]–[3]. A chaotic system is self-synchronizing if it can be decomposed into at least two subsystems: a drive system (transmitter) and a stable response subsystem (receiver) that synchronize when coupled with a common signal. For some synchronized chaotic systems (SCS's), the ability to synchronize is robust. For example, in the Lorenz system, the synchronization is highly robust to perturbations in the drive signal as shown numerically in Section VII. This property leads to some interesting communications applications. For example, the chaotic signal masking technique introduced in [4], [5] appears to be a potentially useful approach to private communications. In a second approach to private communications, the information-bearing waveform is used to modulate a transmitter coefficient. The corresponding synchronization error in the receiver can be used to detect binary-valued bit streams [6], [7].

In a somewhat different context, SCS's can be viewed as performing the role of a nonlinear state space observer. Indeed, the input to a SCS consists of a single component of the transmitter's state vector and produces an estimate of the transmitter's full-dimensional state vector. In the case of noise-free measurements, the asymptotic state estimates are exact, with exponentially fast convergence in the case of the Lorenz system. Structurally, the SCS can be viewed as an open-loop nonlinear observer, since information from feedback signals does not not take part in the synchronization process. To quantify the robustness of the Lorenz SCS to perturbations in the drive signal, we numerically study the ability of the Lorenz SCS to provide meaningful state estimates when driven by a single noisy transmitter component. We then compare the SCS's performance to an extended Kalman filter (EKF) to calibrate the SCS's performance as a nonlinear state estimator.

This paper represents an expanded version of work reported earlier by us [8] and is organized as follows. In Section II, we summarize the concept of synchronized chaotic signals and systems. In Section III, we discuss the electronic circuit implementation of the Lorenz system. In Section IV, a synchronizing receiver circuit that can regenerated the full-dimensional dynamics of the transmitter is discussed and demonstrated. Sections V and VI provide examples of how the transmitter and receiver circuits can be used together for the implementation of new algorithms and approaches to communications. In Section VII, we emphasize a close connection between synchronization in chaotic systems and model-based state estimation using EKFs.

II. Background

The Lorenz system [9] is given by

$$\begin{aligned} \dot{x} &= \sigma(y - x) \\ \dot{y} &= rx - y - xz \\ \dot{z} &= xy - bz \end{aligned} \tag{1}$$

Manuscript received May 23, 1993. This work was supported by the Air Force Office of Scientific Research under Grant Number AFOSR-91-0034-A, the National Science Foundation under Grant DMS-9057433, a subcontract from Lockheed Sanders, Inc. under ONR Contract N00014-91-C-0125, and the Office of Naval Research under Grant N00014-93-1-0686. K. M. Cuomo was supported by the MIT/Lincoln Laboratory Staff Associate Program. This paper was recommended by Guest Editor L. O. Chua.

K. M. Cuomo and A. V. Oppenheim are with the Research Laboratory of Electronics and the Department of Electrical Engineering and Computer Science, Massachusetts Institute of Technology, Cambridge, MA 02139.

S. H. Strogatz is with the Department of Mathematics, Massachusetts Institute of Technology, Cambridge, MA 02139.

IEEE Log Number 9211620.

where σ, r, and b are parameters. As shown by Pecora and Carroll, the Lorenz system is decomposable into two stable subsystems. Specifically, a stable (x_1, z_1) response subsystem can be defined by

$$\begin{aligned} \dot{x}_1 &= \sigma(y - x_1) \\ \dot{z}_1 &= x_1 y - b z_1 \end{aligned} \tag{2}$$

and a second stable (y_2, z_2) response subsystem by

$$\begin{aligned} \dot{y}_2 &= r x - y_2 - x z_2 \\ \dot{z}_2 &= x y_2 - b z_2 \end{aligned} \tag{3}$$

Equation (1) can be interpreted as the drive system, since its dynamics are independent of the response subsystems. Equations (2) and (3) represent dynamical response systems that are driven by the drive signals $y(t)$ and $x(t)$, respectively. The eigenvalues of the Jacobian matrix for the (x_1, z_1) subsystems are both negative, thus, $|x_1 - x|$ and $|z_1 - z| \to 0$ as $t \to \infty$. Also, it can be shown numerically that the Lyapunov exponents of the (y_2, z_2) subsystem are both negative; thus, $|y_2 - y|$ and $|z_2 - z| \to 0$ as $t \to \infty$.

As we show below, the two response subsystems can be used together to regenerate the full-dimensional dynamics that are evolving at the drive system. Specifically, if the input signal to the (y_2, z_2) subsystem is $x(t)$, then the output $y_2(t)$ can be used to drive the (x_1, z_1) subsystem and subsequently generate a "new" $x(t)$ in addition to having obtained, through synchronization, $y(t)$ and $z(t)$. It is important to recognize that the two response subsystems given by (2) and (3) can be *combined* into a single system having a three-dimensional state space. This produces a full-dimensional response system that is structurally similar to the drive system (1). Further discussion of this result is given below in the context of the circuit implementations.

III. The Transmitter Circuit

A direct implementation of (1) with an electronic circuit presents one major difficulty: The state variables in (1) occupy a wide dynamic range with values that exceed reasonable power supply limits. However, this difficulty can be eliminated by a simple transformation of variables. Specifically, for the coefficients σ, r, and b used here, an appropriate transformation is $u = x/10$, $v = y/10$, and $w = z/20$. With this scaling, the Lorenz equations are transformed to

$$\begin{aligned} \dot{u} &= \sigma(v - u) \\ \dot{v} &= r u - v - 20 u w \\ \dot{w} &= 5 u v - b w. \end{aligned} \tag{4}$$

This system, which we refer to as the transmitter, can be more easily implemented with an electronic circuit because the state variables all have similar dynamic range and circuit voltages remain well within the range of typical power supply limits.

An analog circuit implementation of the circuit in the equations in (4) is shown in Fig. 1. The operational amplifiers (1)–(8) and associated circuitry perform the operations of addition, subtraction, and integration. Analog multipliers implement the nonlinear terms in the circuit equations. By

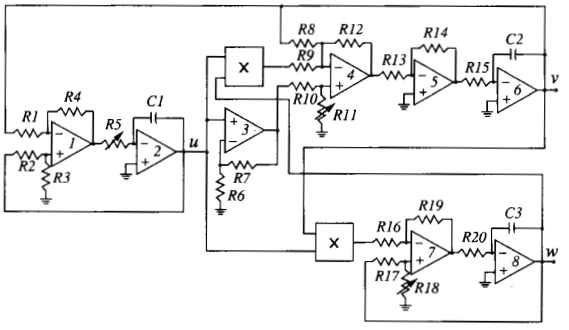

Fig. 1. Lorenz-based chaotic circuit.

applying standard node analysis techniques to the circuit of Fig. 1, a set of state equations that govern the dynamical behavior of the circuit can be obtained. This set of equations is given by

$$\begin{aligned} \dot{u} &= \frac{1}{R_5 C_1}\left[\frac{R_4}{R_1} v - \frac{R_3}{R_2 + R_3}\left(1 + \frac{R_4}{R_1}\right) u\right] \\ \dot{v} &= \frac{1}{R_{15} C_2}\left[\frac{R_{11}}{R_{10} + R_{11}}\left(1 + \frac{R_{12}}{R_8} + \frac{R_{12}}{R_9}\right)\left(1 + \frac{R_7}{R_6}\right) u \right. \\ &\quad \left. - \frac{R_{12}}{R_8} v - \frac{R_{12}}{R_9} u w\right] \\ \dot{w} &= \frac{1}{R_{20} C_3}\left[\frac{R_{19}}{R_{16}} u v - \frac{R_{18}}{R_{17} + R_{18}}\left(1 + \frac{R_{19}}{R_{16}}\right) w\right]. \end{aligned} \tag{5}$$

An examination of these equations shows that the circuit time scale can be easily adjusted by changing the values of the three capacitors C_1, C_2, and C_3 by a common factor. Thus, if a factor of B increase in signal bandwidth is desired, it can be achieved by dividing the three capacitor values by the same factor. In addition, the coefficients σ, r, and b can be independently varied by adjusting the corresponding resistors R_5, R_{11}, and R_{18}. This property allows for a simple way to independently vary the coefficients of the circuit equations. For the component values[1] we have chosen, (5) is equivalent to (4) after rescaling time by a factor of 2505. The resulting coefficients are $\sigma = 16$, $r = 45.6$, and $b = 4$.

To illustrate the chaotic behavior of the transmitter circuit, an analog-to-digital (A/D) data recording system was used to sample the appropriate circuit outputs at 48-kHz rate and with 16-bit resolution. Fig. 2 shows a sample function and averaged power spectrum corresponding to the circuit waveform $u(t)$. The power spectrum is broadband, which is typical of a chaotic signal. Fig. 2(b) also shows the power spectrum obtained from a numerical simulation of the Lorenz equations. As we see, the performance of the circuit and the simulation are consistent. Fig. 3 shows the circuit's chaotic attractor projected onto the uv-plane and uw-plane, respectively. These data were obtained from the circuit using the stereo recording capability of the A/D system to simultaneously sample the x-axis and y-axis signals at a 48-kHz rate and with 16-b resolution. A more detailed analysis of the transmitter circuit is given in [6].

[1] Resistors (kΩ): $R1$, $R2$, $R3$, $R4$, $R6$, $R7$, $R13$, $R14$, $R16$, $R17$, $R19 = 100$ $R5$, $R10 = 49.9$ $R8 = 200$ $R9$, $R12 = 10$ $R11 = 63.4$ $R15 = 40.2$ $R18 = 66.5$ $R20 = 158$ Capacitors (pF): $C1$, $C2$, $C3 = 500$ Op-Amps (1)–(8): LF353 Multipliers: AD632AD.

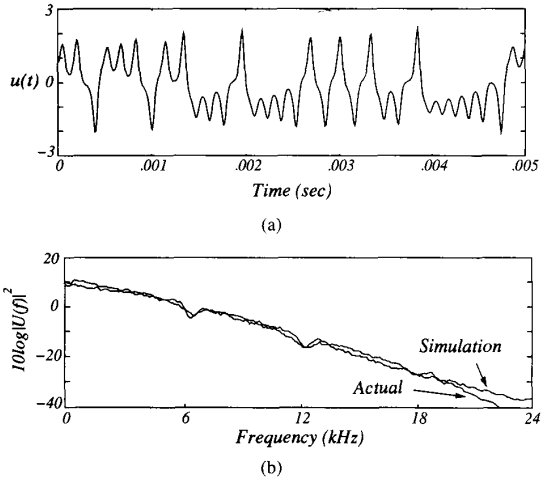

Fig. 2. Circuit data: (a) A sample function of $u(t)$. (b) Averaged power spectrum of $u(t)$.

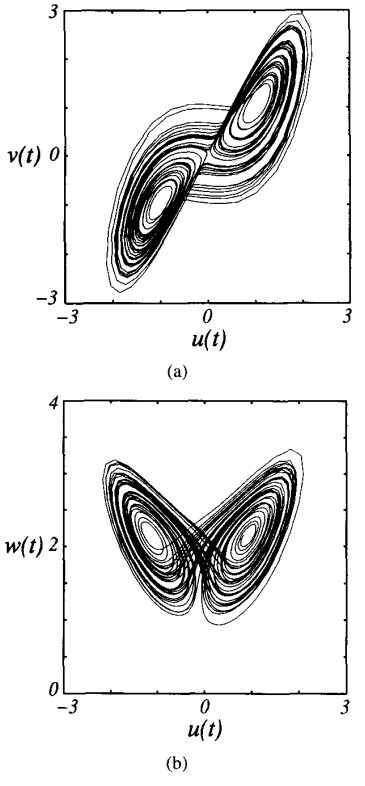

Fig. 3. Circuit data: (a) Chaotic attractor projected onto uv-plane. (b) Chaotic attractor projected onto uw-plane.

IV. The Receiver Circuit

A full-dimensional response system that will synchronize to the chaotic signals at the transmitter (4) is given by

$$\begin{aligned} \dot{u}_r &= \sigma(v_r - u_r) \\ \dot{v}_r &= ru - v_r - 20uw_r \\ \dot{w}_r &= 5uv_r - bw_r \end{aligned} \tag{6}$$

This system is obtained from the transmitter equations by renaming variables from (u, v, w) to (u_r, v_r, w_r) and then substituting $u(t)$ for $u_r(t)$ in the second and third equations. We refer to this system as the receiver in light of some potential communications applications. We denote the transmitter state variables collectively by the vector $\boldsymbol{d} = (u, v, w)$ and the receiver variable by the vector $\boldsymbol{r} = (u_r, v_r, w_r)$ when convenient.

By defining the dynamical errors by $\boldsymbol{e} = \boldsymbol{d} - \boldsymbol{r}$, it is straightforward to show that synchronization in the Lorenz system is a result of stable error dynamics between the transmitter and receiver. Assuming that the transmitter and receiver coefficients are identical, a set of equations that governs the error dynamics is given by

$$\begin{aligned} \dot{e}_1 &= \sigma(e_2 - e_1) \\ \dot{e}_2 &= -e_2 - 20u(t)e_3 \\ \dot{e}_3 &= 5u(t)e_2 - be_3 \end{aligned}$$

The error dynamics are globally asymptotically stable at the origin, provided that σ, b >0. This result follows by considering the 3-D Lyapunov function defined by

$$E(\boldsymbol{e}, t) = \frac{1}{2}\left(\frac{1}{\sigma}e_1^2 + e_2^2 + 4e_3^2\right)$$

The time rate of change of $E(\boldsymbol{e}, t)$ along the trajectories is given by

$$\begin{aligned} \dot{E}(\boldsymbol{e}, t) &= \frac{1}{\sigma}e_1\dot{e}_1 + e_2\dot{e}_2 + 4e_3\dot{e}_3 \\ &= -\left(e_1 - \frac{1}{2}e_2\right)^2 - \frac{3}{4}e_2^2 - 4be_3^2 \end{aligned}$$

Since E is positive definite and $\dot{E}$ is negative definite, Lyapunov's theorem (Theorem 10.2 in [10]) implies that $\boldsymbol{e}(t) \to 0$ as $t \to \infty$. Therefore, synchronization occurs as $t \to \infty$. In the Appendix, we show that the rate of synchronization is exponentially fast. Note also that the transmitter and receiver need not be operating chaotically for synchronization to occur. In [11], a similar Lyapunov argument is given for the synchronization of the (y, z) subsystem of the Lorenz equations.

An electronic implementation of the receiver equations (6) is shown in Fig. 4. Comparison of the receiver circuit with the transmitter circuit of Fig. 1 shows that they are virtually identical, with the only difference being that the drive signal $u(t)$ replaces the receiver signal $u_r(t)$ at a key point in the circuit. The practical advantage of this similarity is that the transmitter and receiver circuits can be built in an identical way, which helps to achieve perfect synchronization between the transmitter and receiver.

To illustrate the synchronization performance of the receiver circuit, the appropriate transmitter and receiver signals were simultaneously recorded using the stereo recording capability of the A/D system. In Fig. 5(a), a plot of the actual circuit outputs $u(t)$ versus $u_r(t)$ is shown. Fig. 5(b) shows a similar plot for the circuit outputs $v(t)$ and $v_r(t)$. The 45° lines indicate that nearly perfect synchronization is achieved and maintained between the transmitter and receiver. The circuit

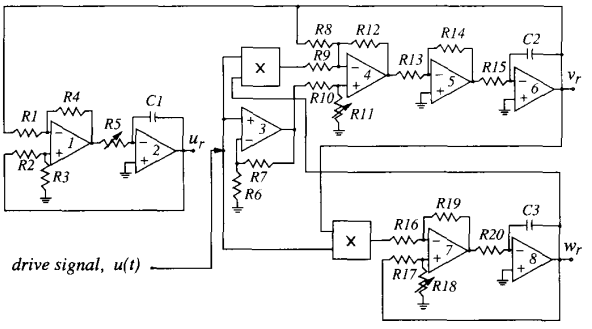

Fig. 4. Synchronizing chaotic receiver circuit.

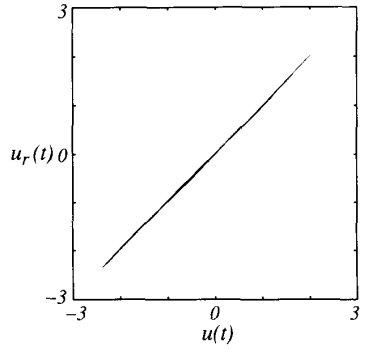

(a)

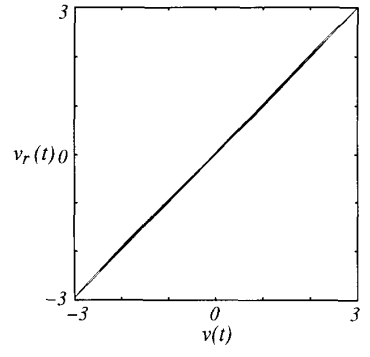

(b)

Fig. 5. Circuit data: Synchronization of transmitter and receiver signals. (a) $u(t)$ versus $u_r(t)$. (b) $v(t)$ versus $v_r(t)$.

outputs shown in Fig. 5 reflect a time span of several minutes, indicating considerable stability of the synchronization.

V. Chaotic Signal Masking

A potential approach to communications applications is based on chaotic signal masking and recovery [4]–[8]. In signal masking, a noiselike masking signal is added at the transmitter to the information-bearing signal $m(t)$, and at the receiver the masking is removed. In our system, the basic idea is to use the received signal to regenerate the masking signal at the receiver and subtract it from the received signal to recover $m(t)$. This can be done with the synchronizing receiver circuit, since the ability to synchronize is found experimentally to be robust,

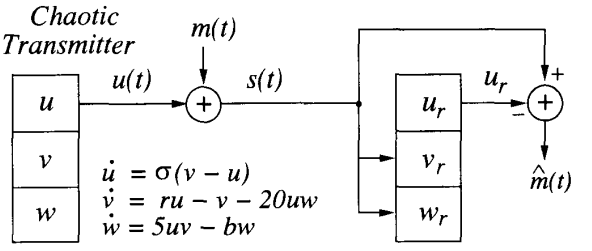

Fig. 6. Chaotic signal masking system.

i.e., is not highly sensitive to perturbations in the drive signal and thus can be done with the masked signal. It is interesting to note that this idea is not restricted to just the Lorenz circuit, but has wider potential. For example, Kocarev *et al.* [12] have also demonstrated our signal masking concept in [4], [5] by using Chua's circuit.

Although there are many possible variations, consider, for example, a transmitted signal of the form $s(t) = u(t) + m(t)$. It is assumed that for masking, the power level of $m(t)$ is significantly lower than that of $u(t)$. The dynamical system implemented at the receiver is

$$\begin{aligned} \dot{u}_r &= 16(v_r - u_r) \\ \dot{v}_r &= 45.6s(t) - v_r - 20s(t)w_r \\ \dot{w}_r &= 5s(t)v_r - 4w_r. \end{aligned}$$

If the receiver has synchronized with $s(t)$ as the drive, then $u_r(t) \simeq u(t)$, and consequently $m(t)$ is recovered as $\hat{m}(t) = s(t) - u_r(t)$. Fig. 6 illustrates the approach.

Using the transmitter and receiver circuits, we demonstrate the performance of this system in Fig. 7 with a segment of speech from the sentence, "He has the bluest eyes." As indicated in Fig. 8, the power spectra of the chaotic masking signal $u(t)$ and the speech are highly overlapping, with an average signal-to-masking ratio of approximately -20 dB. Fig. 7(a) and (b) shows the original speech $m(t)$ and the recovered speech signal $\hat{m}(t)$, respectively. For plotting purposes, these signals were low-pass filtered and downsampled. Clearly, the speech signal was recovered, and was of reasonable quality in informal listening tests.

VI. Chaotic Binary Communications

As a second illustration of the potential use of synchronized chaotic systems in communications, we describe a system to transmit and recover binary-valued bit streams [6]. The basic idea is to modulate a transmitter coefficient with the information-bearing waveform and to transmit the chaotic drive signal. At the receiver, the coefficient modulation will produce a synchronization error between the received drive signal and the receiver's regenerated drive signal with an error signal amplitude that depends on the modulation. Using the synchronization error, the modulation can be detected.

This modulation/detection process is illustrated in Fig. 9. In this figure, the coefficient b of the transmitter (4) is modulated by the information-bearing waveform, $m(t)$. The information is carried over the channel by the chaotic signal $u_m(t)$. The noisy received signal $r(t) = u_m(t) + n(t)$ serves as the

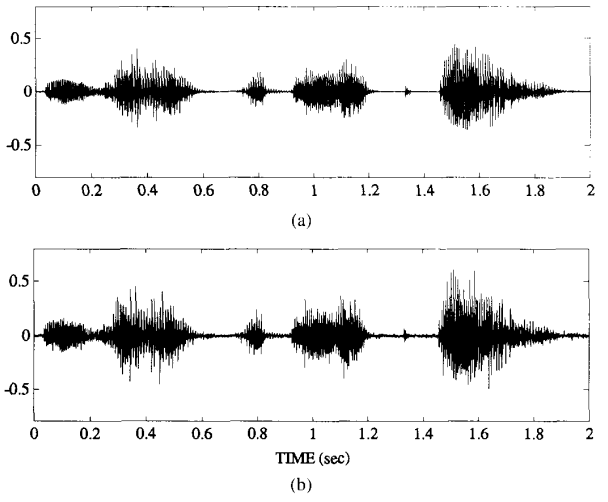

Fig. 7. Circuit data: Speech waveforms. (a) Original. (b) Recovered.

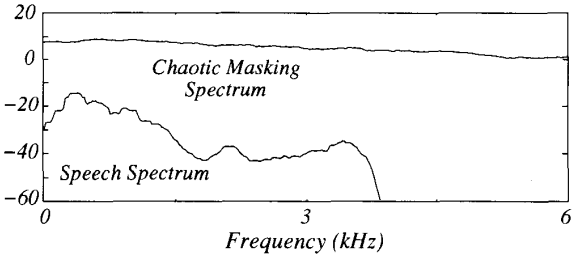

Fig. 8. Circuit data: Power spectra of chaotic masking and speech signals.

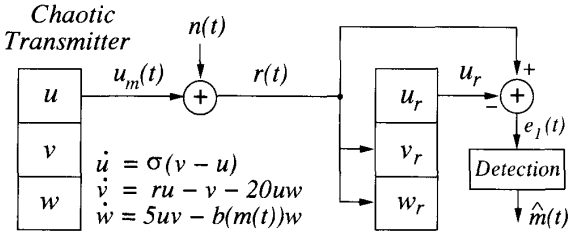

Fig. 9. Chaotic communication system.

driving input to the receiver. At the receiver, the modulation is detected by forming the difference between $r(t)$ and the reconstructed drive signal $u_r(t)$. If we assume that the signal-to-noise ratio (SNR) of $r(t)$ is large, the error signal $e_1(t) = r(t) - u_r(t)$ will have a small average power if no modulation is present. However, if, for example, the information waveform is a binary valued bit stream, with a "1" representing a coefficient mismatch and a "0" representing no coefficient mismatch, then $e_1(t)$ will be relatively large in amplitude during the time period that a "1" is transmitted and small in amplitude during a "0" transmission. The synchronizing receiver can thus be viewed as a form of matched filter for the chaotic transmitter signal $u(t)$.

To illustrate the technique, we use a square-wave for $m(t)$ as shown in Fig. 10(a). The square-wave produces a variation

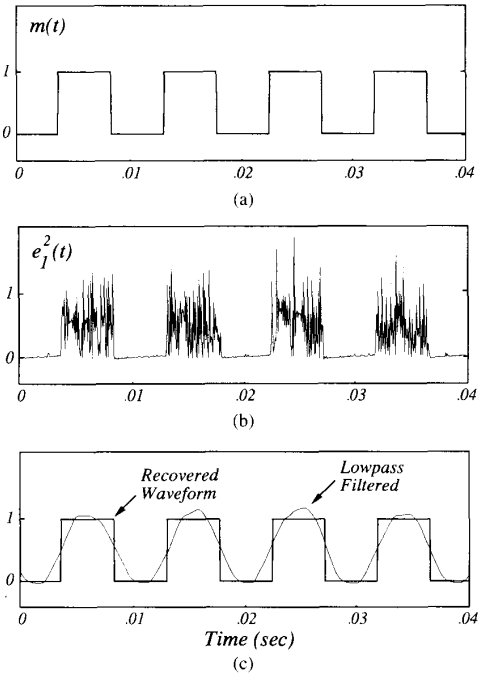

Fig. 10. Circuit data: (a) Modulation waveform. (b) Synchronization error power. (c) Recovered waveform.

in the transmitter coefficient b with the zero-bit and one-bit coefficients corresponding to $b(0) = 4$ and $b(1) = 4.4$, respectively. In [6], we show that the averaged power spectrum of the drive signal with and without the embedded square-wave present are very similar. Fig. 10(b) shows the synchronization error power, $e_1^2(t)$, at the output of the receiver circuit. The coefficient modulation produces significant synchronization error during a "1" transmission and very little error during a "0" transmission. Fig. 10(c) illustrates that the square-wave modulation can be reliably recovered by low-pass filtering the synchronization error power waveform and applying a threshold test. The allowable data rate is, of course, dependent on the synchronization response time of the receiver system. Although we have used a low bit rate to demonstrate the technique, the circuit time scale can be easily adjusted to allow much faster bit rates.

Note that the ability to communicate digital bit streams using this method does not depend on the periodic nature of the square-wave used to demonstrate the technique. The results apply to aperiodic or random bit streams as well. A similar approach using Chua's circuit has also been shown to work by Parlitz *et al.* [13].

VII. Chaotic Synchronization and Nonlinear State Estimation

Synchronized chaotic systems obtain state estimates of a nonlinear deterministic system through the stability of the error dynamics between transmitter and receiver. This seems analogous to using EKF's to produce state estimates of nonlinear probabilistic systems. However, SCS's have an open-loop

structure, and it is not obvious that the SCS can provide robust state estimates when driven by a noisy drive signal. As a step toward further understanding the inherent robustness of the Lorenz SCS, we compare the performance of the Lorenz SCS to an EKF algorithm. The implementation of the EKF is discussed below.

7.1. EKF Implementation

Probabilistic state estimates of the Lorenz system can be obtained with an EKF by expressing the Lorenz system dynamics and measurement model as a dynamical system of the form

$$\begin{aligned} \dot{\boldsymbol{x}} &= \boldsymbol{f}(\boldsymbol{x}(t)) + \boldsymbol{w}(t) \\ y(t) &= H\boldsymbol{x}(t) + v(t) \end{aligned} \tag{7}$$

where $\boldsymbol{w}(t)$ and $v(t)$ represent zero-mean Gaussian white noise sources having spectral intensities $Q(t)$ and $R(t)$, respectively. The process noise $\boldsymbol{w}(t)$, and measurement noise, $v(t)$, are assumed to be uncorrelated, i.e., $E\{\boldsymbol{w}(t)v(\tau)\} = 0$ for all t and τ. For our purposes, the observation matrix H will be constant with only a single nonzero entry. Specifically, since the observations consist of only the noisy x component, the observation matrix H is given by the row vector $H = [1\ 0\ 0]$.

Although, in principle, there should be no process noise term in (7) because the dynamical system that we are studying is given, numerical experiments have shown that the process noise is essential in order to avoid rapid divergence of the Kalman filter state estimates for the Lorenz system. A reason for the divergence becomes clear when considering the form of the EKF corresponding to (7). Specifically, the EKF corresponding to (7) is given by

$$\dot{\hat{\boldsymbol{x}}} = \boldsymbol{f}(\hat{\boldsymbol{x}}(t)) + K(t)[y(t) - H\hat{\boldsymbol{x}}(t)] \tag{8}$$

where $\hat{\boldsymbol{x}}$ is the current state estimate and $K(t)$ is the Kalman gain. Although (8) captures the exact nonlinear dynamics of the system, the state estimates will diverge if the Kalman gain, $K(t)$ becomes small. This follows from the fact that a chaotic system possesses a sensitive dependence on initial conditions, and any error in the current state estimate will be amplified if $K(t)$ is nearly zero.

Linearizing (7) about the current state estimate, the following incremental system, which is valid for small $\delta\boldsymbol{x}(t)$ is obtained as follows:

$$\begin{aligned} \delta\dot{\boldsymbol{x}} &= F(\hat{\boldsymbol{x}}(t))\delta\boldsymbol{x}(t) + \boldsymbol{w}(t) \\ \nu(t) &= H\delta\boldsymbol{x}(t) + v(t) \end{aligned} \tag{9}$$

The time-varying matrix $F(\hat{\boldsymbol{x}}(t))$ corresponds to the Jacobian matrix of the Lorenz system evaluated at the current state estimate. Since (9) represents a linear time-varying system, the Kalman filter error covariance, $P(t)$ is governed by the matrix Riccati equation given below:

$$\begin{aligned} \dot{P} &= F(\hat{\boldsymbol{x}}(t))P(t) + P(t)F^T(\hat{\boldsymbol{x}}(t)) \\ &\quad + Q(t) - P(t)H^T R^{-1}(t)HP(t) \\ K(t) &= P(t)H^T R^{-1}(t). \end{aligned} \tag{10}$$

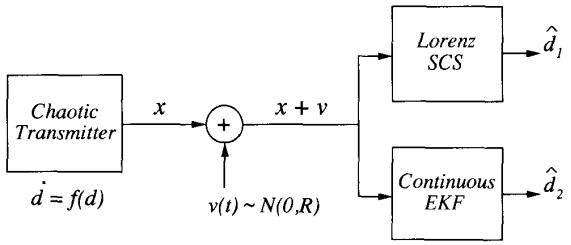

Fig. 11. Numerical experiment.

Equations (8) and (10) determine the EKF state estimates for the Lorenz system. In [6], we also discuss the implementation of a linearized EKF that uses the state estimates from the Lorenz SCS as the nominal trajectory. This approach improves the robustness of the linearized EKF to uncertainties in the transmitter's initial condition.

7.2. Performance Comparisons

In this subsection, we compare the relative performance of the Lorenz SCS and EKF in terms of the input and output SNR. The numerical experiment used to evaluate the output SNR of these state estimators is illustrated in Fig. 11. As indicated, the transmitted signal $x(t)$ corresponds to the x component of the Lorenz system. The input signal to both the SCS and EKF consists of the transmitted chaotic drive signal plus zero-mean Gaussian white noise. Both estimators receive the identical input sample values, i.e., the received signal $x(t) + v(t)$ is simultaneously observed by the SCS and EKF. An initial rest condition is imposed on the SCS, and the EKF is initialized by using the true state of the transmitter at $t = 0$. State estimates were computed numerically for 10 s and the first few seconds of data were discarded to eliminate initial transient effects. The output SNR was then computed for the state estimates from the remaining data.

Fig. 12 shows a performance comparison in terms of input/output SNR. The solid curves correspond with state estimates from the EKF, and the dashed curves correspond with state estimates from the SCS. The performance of the SCS and EKF are comparable over a wide range of input SNR's. A threshold effect is evident for both the SCS and EKF at low-input SNR's. Above the threshold, however, the normalized error in the synchronization of each state variable is approximately 10 db less than the normalized error in the drive signal $x(t)$. We also point out that the SCS is able to provide meaningful state estimates when starting from any initial condition. The EKF, however, requires accurate initial conditions, or the state estimates may rapidly diverge.

7.3. Modeling Errors

As a matter of practical significance, we numerically evaluate the sensitivity of the Lorenz SCS and EKF to coefficient modeling errors at the receiver. For this experiment, the transmitter coefficients are held fixed, and all of the receiver coefficients are treated as uniformly distributed random variables having mean values equal to the corresponding transmitter coefficient. The variance of the receiver coefficients

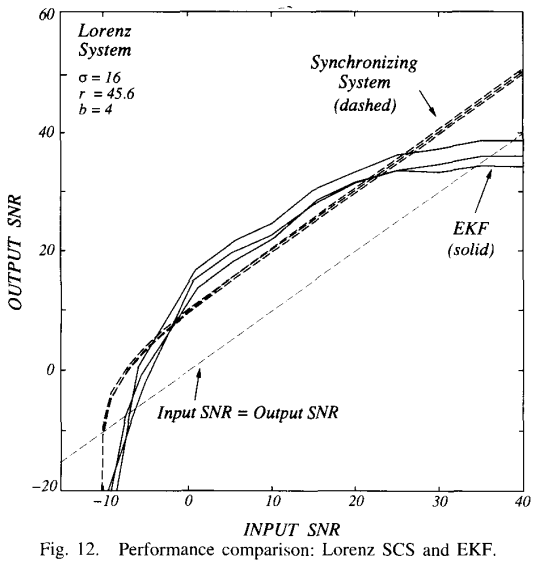

Fig. 12. Performance comparison: Lorenz SCS and EKF.

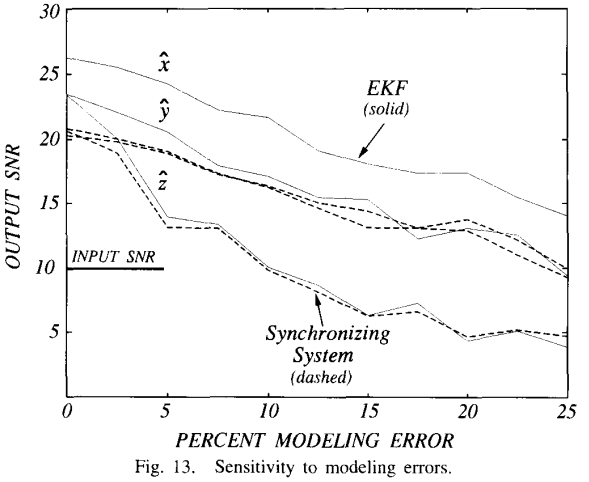

Fig. 13. Sensitivity to modeling errors.

depend on the percentage modeling error being tested, where modeling error is defined as the ratio of the standard deviation to the mean value of the receiver coefficients.

Fig. 13 shows a sensitivity comparison between the Lorenz SCS and EKF state estimators, where the input signal corresponds to the transmitters's noisy x component having a 10-dB input SNR. These curves were generated by selecting receiver coefficients from ten independent trials having the indicated error. The slopes of these curves indicate that the sensitivity of these two state estimators is nearly the same over the range of modeling errors tested.

APPENDIX

To show that $\boldsymbol{e}(t)$ decays at least exponentially fast, let $V = \frac{1}{2}e_2^2 + 2e_3^2$. Then, V decays at least exponentially fast because $\dot{V} = -e_2^2 - 4be_3^2 \leq -kV$ for any $k < \min(2, 2b)$. Integration then yields $0 \leq V(t) \leq V_0 e^{-kt}$. Next, observe that $\frac{1}{2}e_2^2 \leq V \leq V_0 e^{-kt}$ so that $e_2(t) \leq (2V_0)^{1/2} e^{-kt/2}$. Similarly, $e_3(t) \leq O(e^{-kt/2})$. Finally, integration of $\dot{e}_1 = \sigma(e_2 - e_1)$, combined with $e_2(t) \leq O(e^{-kt/2})$, implies that $e_1(t) \leq \max\{O(e^{-\sigma t}), O(e^{-kt/2})\}$. Thus, all components of $\boldsymbol{e}(t)$ decay at least exponentially fast.

ACKNOWLEDGMENT

The authors thank S. H. Isabelle, Prof. A. S. Willsky, and Prof. G. W. Wornell for many helpful discussions during various stages of this work.

REFERENCES

[1] L. M. Pecora and T. L. Carroll, "Synchronization in chaotic systems," *Phys. Rev. Lett.*, vol. 64, pp. 821–824, Feb. 1990.
[2] ——, "Driving system with chaotic signals," *Phys. Rev. A.*, vol. 44, pp. 2374–2383, Aug. 1991.
[3] T. L. Carroll and L. M. Pecora, "Synchronizing chaotic circuits," *IEEE Trans. Circuits Syst.*, vol. 38, pp. 453–456, Apr. 1991.
[4] K. M. Cuomo, A. V. Oppenheim, and S. H. Isabelle, "Spread spectrum modulation and signal masking using synchronized chaotic systems," *MIT Res. Lab. Electron. TR 570*, Feb. 1992.
[5] A. V. Oppenheim, G. W. Wornell, S. H. Isabelle, and K. M. Cuomo, "Signal processing in the context of chaotic signals," in *Proc. IEEE ICASSP*, Mar. 1992.
[6] K. M. Cuomo and A. V. Oppenheim, "Synchronized chaotic circuits and systems for communications," *MIT Res. Lab. Electron. TR 575*, Nov. 1992.
[7] ——, "Chaotic signals and systems for communications," *Proc. IEEE ICASSP*, Mar. 1993.
[8] K. M. Cuomo and A. V. Oppenheim, "Circuit implementation of synchronized chaos with applications to comunications," *Phys. Rev. Lett.*, vol. 71, no. 1, p. 65–68, July 1993.
[9] E. N. Lorenz, "Deterministic nonperiodic flow," *J. Atmospheric Sci.*, vol. 20, pp. 130–141, Mar. 1963.
[10] D. W. Jordon and P. Smith, *Nonlinear Ordinary Differential Equations*. New York: Oxford University Press. 1987, 2nd ed.
[11] R. He and P. G. Vaidya, "Analysis and synthesis of synchronous periodic and chatoic systems," *Phys. Rev. A.*, vol. 46, pp. 7387–7392, Dec. 1992.
[12] L. Kocarev, K. Halle, K. Eckert, and L. Chua, "Experimental demonstration of secure communications via chaotic synchronization," *Int. J. Bifurcation Chaos*, vol. 2, pp. 709–713, Sept. 1992.
[13] U. Parlitz, L. Chua, L. Kocarev, K. Halle, and A. Shang, "Transmission of digital signals by chaotic synchronization," *Int. J. Bifurcation Chaos*, vol. 2, pp. 973–977, Dec. 1992.

Kevin M. Cuomo (S'83–M'86) received the B.S. (magna cum laude) and M.S. degrees in electrical engineering from the State University of New York at Buffalo in 1984 and 1986, respectively. Since 1991, he has been pursuing the Ph.D. degree in electrical engineering at the Massachusetts Institute of Technology.

From 1986 to 1988, he was a research staff member at Calspan Corporation, Buffalo, NY. In 1988, he joined the MIT Lincoln Laboratory, where he is currently a staff member specializing in the development of advanced radar imaging methods. He is currently a member of the MIT Lincoln Laboratory Staff Associate Program.

While attending SUNY at Buffalo, he was awarded Departmental Honors (1984) and was the recipient of a University Fellowship (1984–1986) and a Hughes Fellowship (1983–1986). He is also a member of Tan Beta Pi, Eta Kappa Nu, and Sigma Xi.

Alan V. Oppenheim (S'57–M'65–SM'71–F'77) received the S.B. and S.M. degrees in 1961 and the Sc.D. degree in 1964, all in electrical engineering, from the Massachusetts Institute of Technology, Cambridge, MA.

In 1964, he joined the faculty at MIT, where he is currently distinguished Professor of Electrical Engineering. From 1978 to 1980, he was Associate Head of the Data Systems Division at MIT Lincoln Laboratory. Since 1977, he has also been a Guest Investigator at the Woods Hole Oceanographic Institution, Woods Hole, MA. He is the author of several widely used textbooks on digital signal processing.

Dr. Oppenheim has been a Guggenheim Fellow, a Sackler Fellow, and has held the Cecil H. Green Distinguished Chair in Electrical Engineering and Computer Science. He has also received a number of awards for outstanding research and teaching, including the 1988 IEEE Education Medal, and is an elected member of the National Academy of Engineering. He is also a member of Tau Beta Pi, Eta Kappa Nu, and Sigma Xi.

Steven H. Strogatz is an Associate Professor of applied mathematics at the Massachusetts Institute of Technology. After receiving the A.B. degree (summa cum laude) in mathematics from Princeton University in 1980, he spent two years as a Marshall Scholar at Trinity College, Cambridge University. He received the Ph.D. degree in applied mathematics from Harvard University in 1986.

His research deals with applications of dynamical systems in physics and biology, especially problems involving synchronization of coupled nonlinear oscillators.

Dr. Strogatz was awarded a Presidential Young Investigator grant from the National Science Foundation in 1990.